Pergamon

0301-9322(94)00062-X

Int. J. Multiphase Flow Vol. 21, No. 3, pp. 529–542, 1995

0301-9322/95 $9.50 + 0.00

A NUMERICAL STUDY OF THREE-DIMENSIONAL COMBINED BUOYANCY AND THERMOCAPILLARY CONVECTION

M. BEHNIA†, F. STELLA and G. GUJ

Dipartimento di Meccanica e Aeronautica, Università di Roma *La Sapienza*, Via Eudossiana 18, 00184 Roma, Italy

(Received 27 July 1992; in revised form 25 July 1994)

Abstract—In the present study we consider the problem of combined buoyancy and thermocapillary convection in an upright cube with a top free surface. All other walls are considered to be solid and impermeable. The side walls are at uniform but different temperatures, whilst all other surfaces are adiabatic. The top surface deformation and interactions with the gaseous phase above are neglected.

The Navier–Stokes, continuity and energy equations are cast in the velocity–vorticity formulation. The governing equations are discretized by using finite difference approximations. The solution procedure consists of a three level Alternating Direction Implicit (ADI) scheme. In order to save on computational cost, the equations were marched in time using the false transient technique. A typical $81 \times 81 \times 61$ uniform staggered mesh has been used in the numerical computations. All computations were performed in double precision on a work-station.

Results are presented for a typical fluid with a moderate Prandtl number (i.e. $Pr = 7$). The effects of positive and negative Marangoni number on the three-dimensional convection at different Rayleigh numbers will be considered and discussed.

1. INTRODUCTION

In the last 50 years or so the problem of natural convection in enclosures, due to its many industrial and engineering applications, has been studied quite extensively. Natural convection in many systems is the most important and quite often the dominant mode of heat or mass transfer (Gebhart *et al.* 1988). In a number of these applications such as crystal growth, ice making, glass manufacturing, welding, metallurgy, chemical processing and others, the liquid is exposed to a gaseous phase (i.e. free surface condition). The presence of this type of boundary can not only alter the flow field and heat transfer characteristics but may also prove to have an impact on the process because of surface tension variations (Smith & Davis 1983; Bergman & Ramadhyani 1986). In general, for most liquids there is a variation of the surface tension with temperature. As a result, the interface between two immiscible fluids which is subjected to a temperature gradient can initiate a bulk flow due to surface tension variations. In an open differentially heated cavity the motion can be induced due to different and sometimes opposing effects, i.e. buoyancy and thermocapillary convection. The former is related to the non-conservative body forces whereas the latter (normally referred to as thermocapillary flow) is directly related to the surface tension gradient with respect to temperature which acts as a force applied to the boundary (Scriven & Sterling 1960). This flow which is due to temperature gradients parallel to the free surface is known as thermocapillary convection whereas surface tension driven convection due to a temperature gradient applied normally to the free surface is referred to as Marangoni convection (Lebon 1984). However, in the literature the terms thermocapillary and Marangoni convection are sometimes interchanged (e.g. Villers & Platten 1987).

The surface tension variation with temperature can be either an increasing or decreasing, linear or nonlinear function (Villers & Platten 1985; Limbourg-Fontaine *et al.* 1985). As the gradient can be positive or negative, depending on the fluid, thermocapillary convection can either augment or oppose buoyancy driven convection. This in turn has an effect on the flow and heat transfer characteristics (Bergman & Keller 1988).

†Visiting Professor from the University of New South Wales, Sydney, Australia.

The importance of Marangoni effects on buoyancy driven convective flows has been reviewed by several researchers (e.g. Schwabe 1981; Myshkis *et al.* 1986). A number of experimental and numerical studies are cited in these references and are not repeated here. In general, both experimental and numerical studies are categorised by the fluid Prandtl number (Pr). Only a few studies have concentrated on moderate Pr fluids (Pétré *et al.* 1983; Bergman & Ramadhyani 1986; Platten *et al.* 1988) that has on the contrary several practical applications because many organic liquids and mixtures fall into this category.

With the increasing importance of material processing and advancement of space studies, more and more attention has been focused on the combined Marangoni and buoyancy driven convection in the last decade. Further, due to the ever increasing speed of computers and cost effectiveness of computational fluid dynamics, most of the recent studies have been numerical and in general two dimensional. Such computations allow a basic understanding of the flow fluid and thermal structures as well as determining the importance of the interaction between buoyancy and thermocapillary mechanisms. However, three dimensional effects can be a very important factor in determining the flow and thermal structures (Afrid & Zebib 1990; Babu & Korpela 1990). Further, a very important feature of these types of flows is the transition to unsteadiness (oscillatory motion) which is primarily three dimensional (Smith & Davis 1983; Zebib *et al.* 1985; Davis 1987). Correct prediction of such transition is subject to the solution of three-dimensional equations (Afrid & Zebib 1990) and may have a very crucial impact on relevant applications (e.g. crystal growth). Recently Babu & Korpela (1990) numerically studied the problem of three-dimensional thermocapillary convection (in the absence of buoyancy) in a cube. They performed a limited number of computations for Pr of 0.1 and 0.01. This study was a continuation of the axi-symmetric thermocapillary flow in a cylinder (Ramanan & Korpela 1990) stimulated by applications in welding. There appears to be very little experimental and numerical work done on the combined Marangoni and buoyancy convection in a three-dimensional cavity. The experiments have been primarily concerned with two-dimensional measurements (e.g. Villers & Platten 1987) and have therefore revealed very little information on the structure and behaviour of the three-dimensional flow. In the present study we consider this problem in an upright cube with a top free surface and all the other walls solid. Two of the opposing side walls are at uniform but different temperatures, whilst all other surfaces are perfectly insulated. The top surface deformation and interaction with the gaseous phase above are neglected. The surface tension variation is considered to be a linear function of temperature only. Results have been obtained for a fluid with $\mathrm{Pr} = 7$ and different Rayleigh (Grashof) numbers as well as a range of both positive and negative Marangoni numbers. Because of a lack of three-dimensional experimental data, we have not been able to make direct comparisons between our computations and measurements.

2. VORTICITY–VELOCITY FORMULATION OF NAVIER–STOKES EQUATIONS

The non-dimensional laminar flow Navier–Stokes equation with Boussinesq approximation in an incompressible Newtonian fluid is:

$$\frac{1}{\mathrm{Pr}}\frac{\partial \mathbf{u}}{\partial t} + \frac{1}{\mathrm{Pr}}(\mathbf{u}\cdot\nabla)\mathbf{u} = -\frac{1}{\mathrm{Pr}}\nabla p + \nabla^2\mathbf{u} - \mathrm{Ra}\,\theta\frac{\mathbf{g}}{g} \qquad [1]$$

in which

$$\mathrm{Ra} = \frac{g\beta\Delta T H^3}{\kappa\nu}$$

and

$$\mathrm{Pr} = \frac{\nu}{\kappa}$$

are the Rayleigh and Prandtl numbers respectively, where g is the modulus of the gravitational acceleration, β is the coefficient of thermal expansion, H and ΔT are the distance and temperature

difference between the hot and cold surfaces respectively, κ is the thermal diffusivity, ν is the kinematic viscosity and the reference velocity is K/H.

The Lagrange form of the advective term, which is more suitable for deriving the vorticity transport equation, is obtained from the following vectorial identity

$$\mathbf{u} \times (\nabla \times \mathbf{u}) = \tfrac{1}{2}\nabla(\mathbf{u} \cdot \mathbf{u}) - (\mathbf{u} \cdot \nabla)\mathbf{u} \qquad [2]$$

and substituting the vorticity definition,

$$\boldsymbol{\omega} = \nabla \times \mathbf{u} \qquad [3]$$

in [1], the following form of the Navier–Stokes equation follows:

$$\frac{1}{\mathrm{Pr}}\frac{\partial \mathbf{u}}{\partial t} + \frac{1}{\mathrm{Pr}}\frac{1}{2}\nabla(\mathbf{u} \cdot \mathbf{u}) + \frac{1}{\mathrm{Pr}}(\boldsymbol{\omega} \times \mathbf{u}) = -\frac{1}{\mathrm{Pr}}\nabla p + {}^{2}\mathbf{u} - \mathrm{Ra}\,\theta\frac{\mathbf{g}}{g}. \qquad [4]$$

The vorticity transport equation in conservative form is then derived by applying the curl operator to both terms of [4]:

$$\frac{1}{\mathrm{Pr}}\frac{\partial \boldsymbol{\omega}}{\partial t} + \frac{1}{\mathrm{Pr}}\nabla \times (\boldsymbol{\omega} \times \mathbf{u}) = \nabla^2\boldsymbol{\omega} - \mathrm{Ra}\,\nabla \times \left(\theta\frac{\mathbf{g}}{g}\right) \qquad [5]$$

The proposed three-dimensional conservative form of the convective term is analogous to the well known two-dimensional one (Guj & Stella 1988). The velocity equations are derived by applying the curl operator to the vorticity definition [3]:

$$\nabla \times \boldsymbol{\omega} = \nabla \times (\nabla \times \mathbf{u}) = \nabla(\nabla \cdot \mathbf{u}) - \nabla^2\mathbf{u} \qquad [6]$$

and using the continuity equation for incompressible flows, i.e. $\nabla \cdot \mathbf{u} = 0$, the following kinematic relation is obtained:

$$\nabla^2\mathbf{u} = -\nabla \times \boldsymbol{\omega}. \qquad [7]$$

The energy transport equation in terms of temperature is:

$$\frac{\partial \theta}{\partial t} + (\mathbf{u} \cdot \nabla)\theta = \nabla^2\theta. \qquad [8]$$

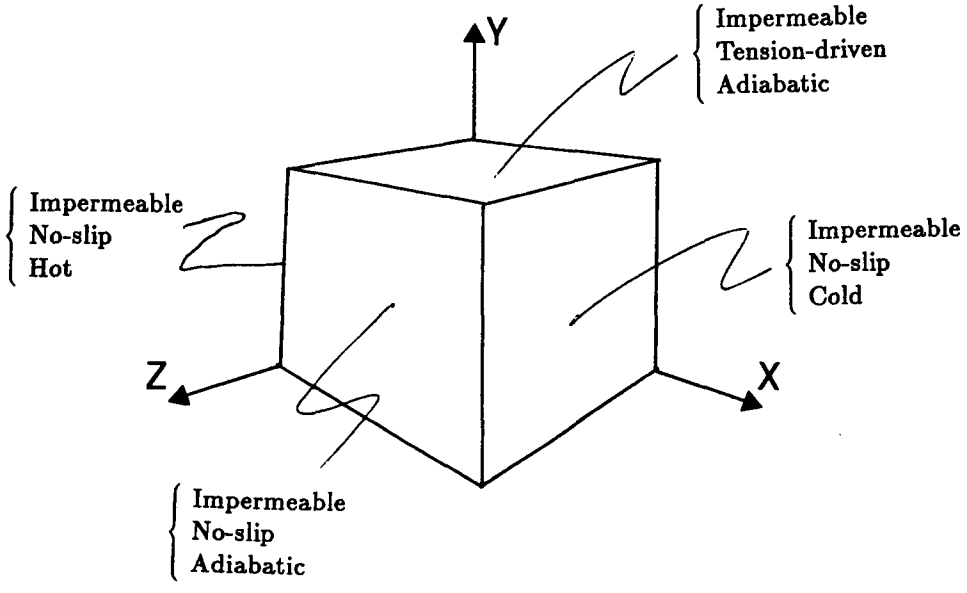

Figure 1. Sketch of the cubic cavity and boundary conditions.

3. BOUNDARY CONDITIONS

All boundaries of the cubical box (see figure 1), except the top free surface, are assumed to be impermeable and at rest. The top free surface is considered to be flat, corresponding to a fluid with a contact angle of 90°. This assumption is not very restrictive. Further, it has been shown that this assumption does not affect the flow structure (Zebib *et al.* 1985; Babu & Korpela 1990). Nonetheless, the shape of the free surface can be calculated *a posteriori* as shown in the previous references. The kinematic boundary conditions on the rigid walls are:

$$\mathbf{u} = 0 \quad \begin{cases} x_1 = 0, 1 \\ x_2 = 0 \\ x_3 = 0, 1 \end{cases} \tag{9}$$

while on the free surface ($x_2 = 1$)

$$u_2 = 0 \tag{10}$$

$$\partial u_i / \partial x_2 = -\mathrm{Ma}\, \partial\theta / \partial x_i \quad i = 1, 3 \tag{11}$$

where the Marangoni number Ma is defined as usual:

$$\mathrm{Ma} = \left(\frac{\partial\sigma}{\partial T}\right)\frac{\Delta T}{\rho\kappa\nu} \tag{12}$$

here ρ and σ are density and surface tension respectively and we assume $\partial\sigma/\partial T$ is constant. The minus sign in the boundary condition on the free surface is introduced because with this notation convection due to positive Ma augments the present buoyancy convection whereas negative Ma opposes natural convection. The boundary conditions for vorticity are obtained directly from the definition of vorticity [3].

The temperature boundary conditions are

$$\frac{\partial\theta}{\partial n} = 0 \quad \begin{cases} x_2 = 0, 1 \\ x_3 = 0, 1 \end{cases} \tag{13}$$

on the adiabatic lateral and bottom walls and on the top free surface, where n is the normal direction and

$$\begin{aligned} \theta &= 1 \quad x_1 = 0 \\ \theta &= 0 \quad x_1 = 1 \end{aligned} \tag{14}$$

on the isothermal vertical walls. Figure 1 sketches the boundary conditions and locations and directions of the axes.

4. DISCRETIZED SCHEME

4.1. Time integration and iterative procedure

The solenoidality constraints on velocity and vorticity fields require a coupled solution of the system given by [5], [7] and [8], with the respective boundary conditions. Unfortunately, the number of the unknowns in three-dimensional domains discourages the use of a direct solver for the entire problem. Furthermore, an iterative procedure is nonetheless required due to the presence of the nonlinear convective terms in [5] and [8].

In the proposed numerical method the necessary iterative procedure for obtaining the steady state solution is based on a false transient method (Mallinson & de Vahl Davis 1973), which solves the parabolic equations [5] and [8] and the following parabolized version of the velocity equation:

$$\alpha\frac{\partial\mathbf{u}}{\partial t} - \nabla^2\mathbf{u} - \nabla\times\boldsymbol{\omega} = \mathbf{0} \tag{15}$$

where α is a relaxation parameter. In this solution procedure it is obvious that steady state is reached when the time derivatives approach zero. The time integration procedure is performed

Table 1. Mesh sensitivity analysis (Ra = 1000, Ma = 1000 and Pr = 7)

Mesh	$\|u_1\|_{max}$	$\|u_2\|_{max}$	$\|u_3\|_{max}$
21 × 21 × 21	27.87	21.70	4.56
41 × 41 × 41	28.37	21.81	4.91
81 × 81 × 61	28.55	21.88	5.12

using a simple ADI algorithm on each scalar equation (Samarskii & Andreyev 1963). The proposed ADI method is particularly suited for efficient computations both on vector and parallel computers (Stella & Guj 1992). It is noted that using the method of false transient is computationally cost effective, however the transient solution is lost. With slight modification to the method it is possible to obtain the transient behaviour and study unsteady or oscillatory problems. In fact, using this method very accurate solutions to the problem of oscillatory natural convection in a cavity have been obtained by Behnia *et al.* (1990) and Behnia & de Vahl Davis (1990).

4.2. Spatial discretization

The finite difference approximations of the governing equations are derived by replacing the time derivatives with forward differences and the spatial first and second order derivatives with second order central differences.

The staggering of the variable location is chosen not only to obtain the maximum accuracy of the discretized derivatives, but also to ensure the conservation of mass and vorticity at the discrete

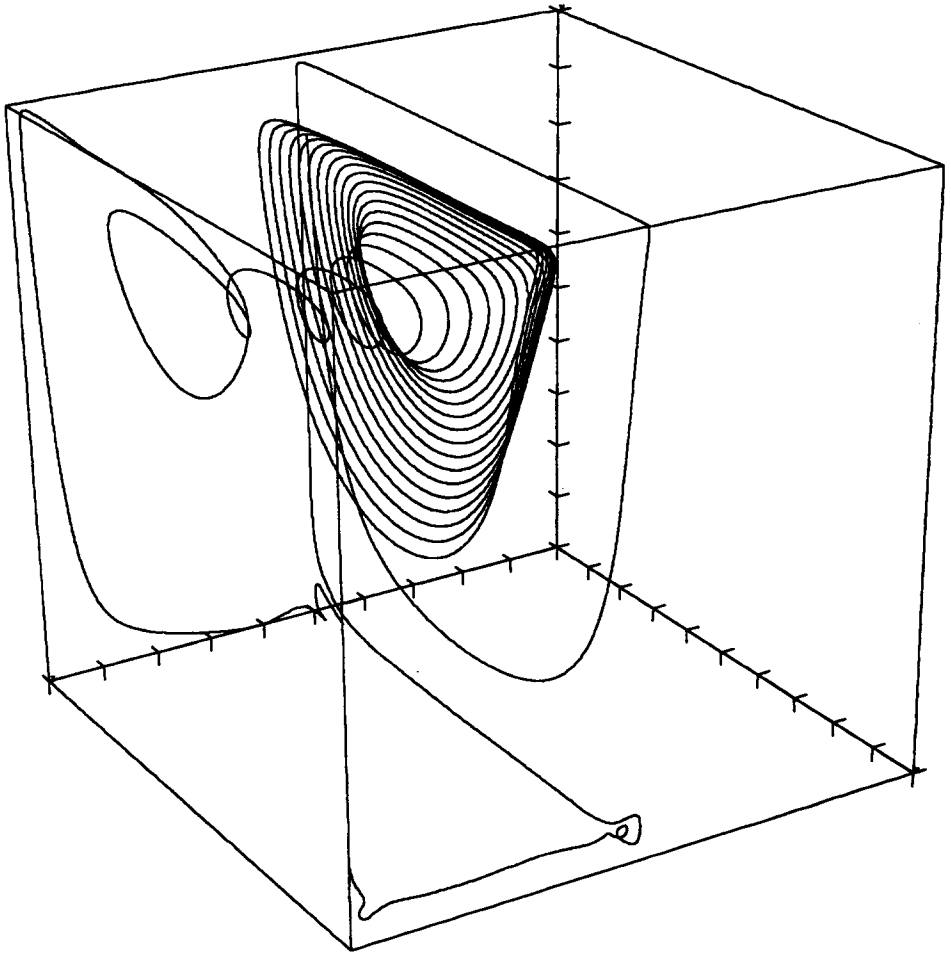

Figure 2. Flow structure (Ra = 0, Ma = 1000).

level. By analogy with the two-dimensional case (Guj & Stella 1988), it is possible to satisfy mass conservation, to roundoff error level, if the velocity component u_i is located at the middle of the face of the computational cell which is normal to x_i. In this way, the computational molecule may be regarded as a control volume for mass conservation, which is satisfied to round-off error level on each individual computational cell. Similarly, each vorticity component is located at the mid-point of the edge of the cell parallel to the corresponding axis, and a control volume, shifted by a half spatial step in the three directions, is considered to impose the solenoidality of vorticity. Furthermore, the proposed variable location guarantees the maximum of accuracy in the computation of the right-hand side of [7] using a two points formula.

The correct location of the variables of the problem is found by using the general rule of applying the discrete operators. This rule can not be used in a straightforward manner in discretizing the nonlinear terms. In fact, the staggered variables location is not sufficient to ensure the solenoidality of vorticity field in the *discrete form*. It is also essential that, in obtaining the finite difference approximations of the advective terms, $\nabla \times (\omega \times \mathbf{u})$, the required needed averaging is performed on the product $(\omega \times \mathbf{u})$ and not on the individual ω and $\mathbf{u}$ terms.

5. RESULTS

Several numerical test cases have been computed in order to study the various effects of surface tension and buoyancy on the flow structure. As discussed previously the sign of Marangoni number (Ma) has been chosen in such a way that positive Ma effect increases the buoyancy convection and negative Ma opposes it.

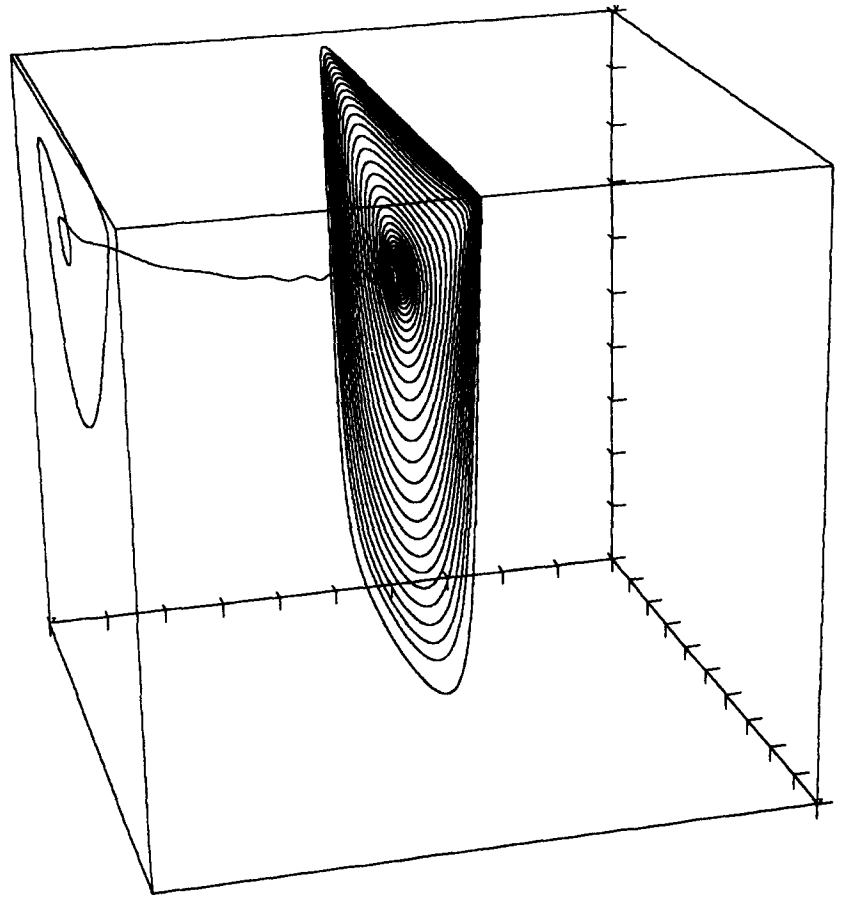

Figure 3. Flow structure (Ra = 1000, Ma = 1000).

A preliminary mesh sensitivity analysis has been performed at Ra = 1000 and Ma = 1000 in order to evaluate the accuracy of the computational code we used. Results are shown in table 1. It is noted that there is a variation of 0.6 and 0.4% in the maximum of u_1 and u_2 component of velocity between $41 \times 41 \times 41$ and $81 \times 81 \times 61$ grids. The relatively higher variation (4.1%) found on u_3 component has to be explained with the smaller absolute value of this numerical quantity compared with the magnitude of u_1 and u_2.

The basic mechanisms related with the two phenomena involved in these types of flow are strongly different from each other. Thermocapillary effect is a surface tension driven phenomenon and hence it primarily affects the flow near the free (top) surface of the container. Natural convection, on the contrary, is caused by temperature gradients present in the body of the fluid and for this reason its effects are distributed in the bulk of the flow field. One of the aims of the present work is to study how these two effects are interacting at the different values of the chosen parameters (i.e. Ra = 0, 1000 and 10,000 with Ma = −1000, 0 and 1000). A number of different cases are computed and the results for each case are presented and discussed below. One of the difficulties in the three-dimensional studies is the presentation of the large quantity of data produced. It is either possible to present the flow velocity data on two-dimensional planes or in the full three-dimensional domain. Here, we have chosen to use a three-dimensional particle tracking technique for visualization of the computed flow structures.

5.1. Flow structure

Case (A): Ra = 0, Ma = 10^3. In this test case, only the effects of surface tension are present, the Rayleigh number being set to zero. The flow is driven due to the effect of velocity gradients on the top surface. For this reason the overall structure of the flow is similar to that of a three-dimensional driven cavity. The flow is mainly developed near this surface and a large vortex

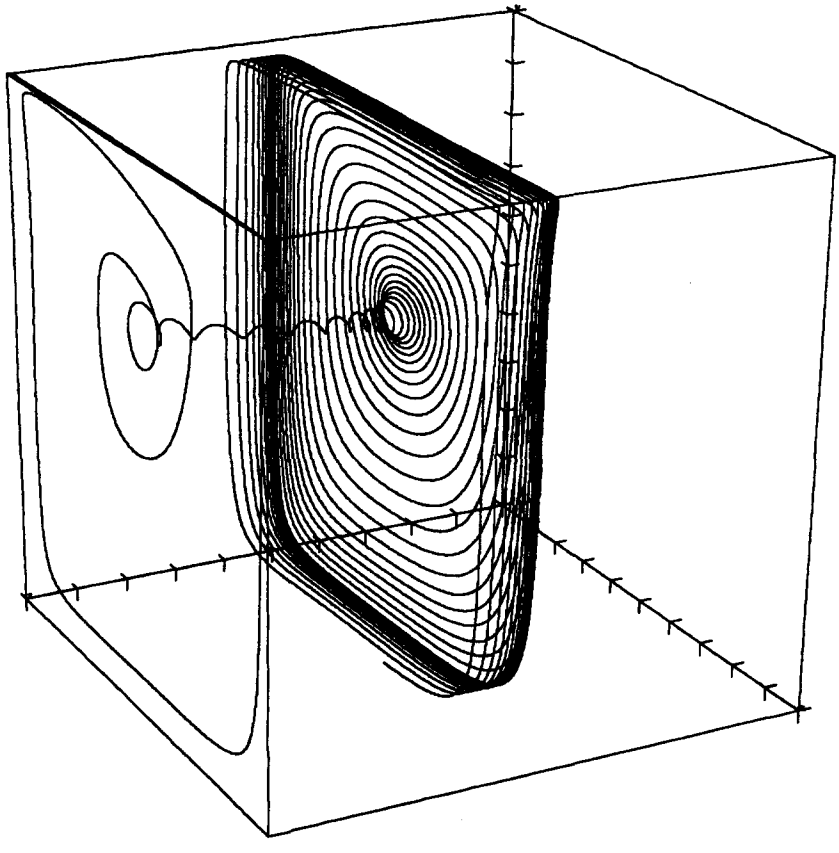

Figure 4. Flow structure (Ra = 10,000, Ma = 1000).

located in the upper region of the cavity is the dominant flow structure as shown in figure 2. In the core of the vortex the flow is spiralling from the end-wall to the middle of the cavity and a reverse flow slowly spiralling from the middle of the cavity to the end-wall is present on the external side of the vortex itself. In addition to this flow structure, two thin secondary vortices are also present in the vicinity of the two edges on the bottom of the cavity moving from the cavity centre to the end-walls.

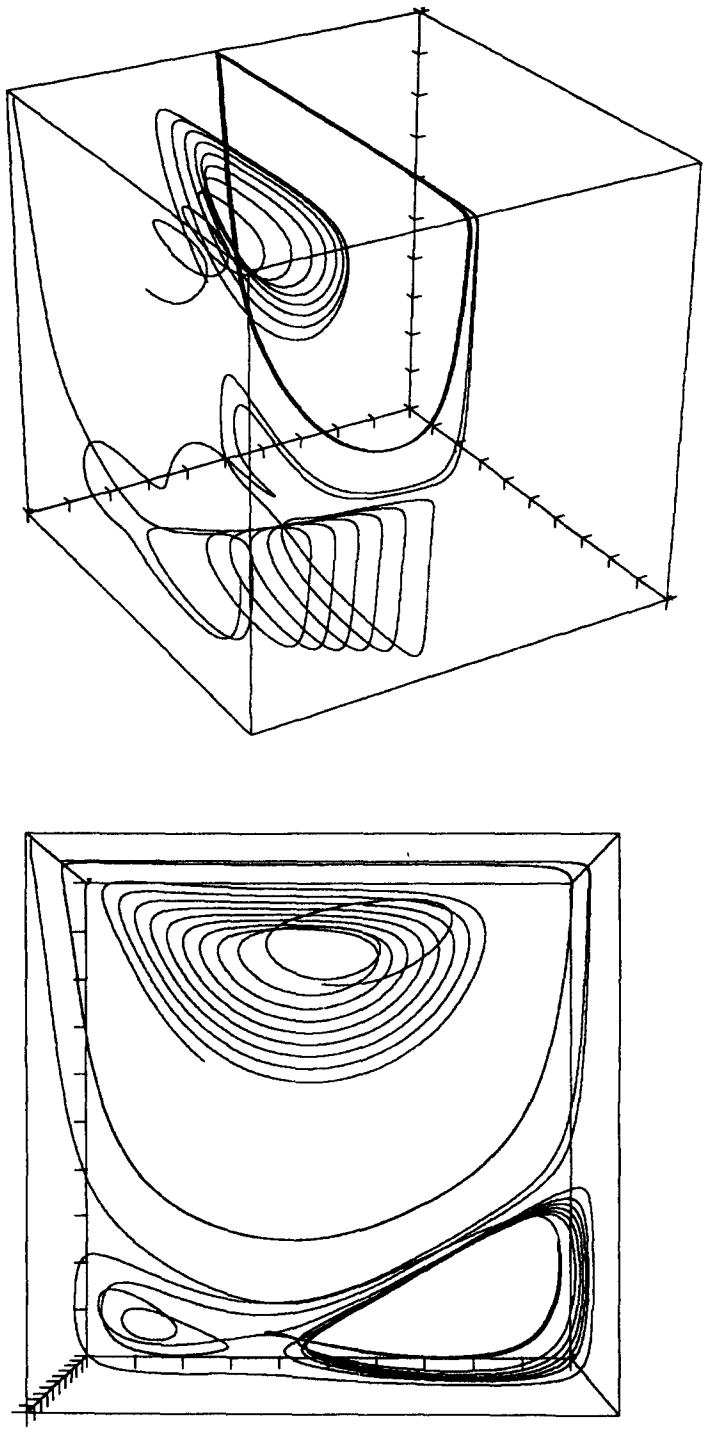

Figure 5. Flow structure (Ra = 1000, Ma = −1000).

Case (B): Ra = 10^3, Ma = 10^3 and Case (C): Ra = 10^4, Ma = 10^3. In these two cases the effect of buoyancy on the flow field is added to the positive Marangoni one. So the flow structure is still constituted by a single large main recirculation. Due to the effect of buoyancy forces, that are distributed in the bulk of the cavity, the main vortex is stronger than in case (A) and encompasses almost completely the entire flow domain (figures 3 and 4). Furthermore, as Ra increases the position of the centre of the main vortex moves down, closer to the cavity mid-plane. This is due

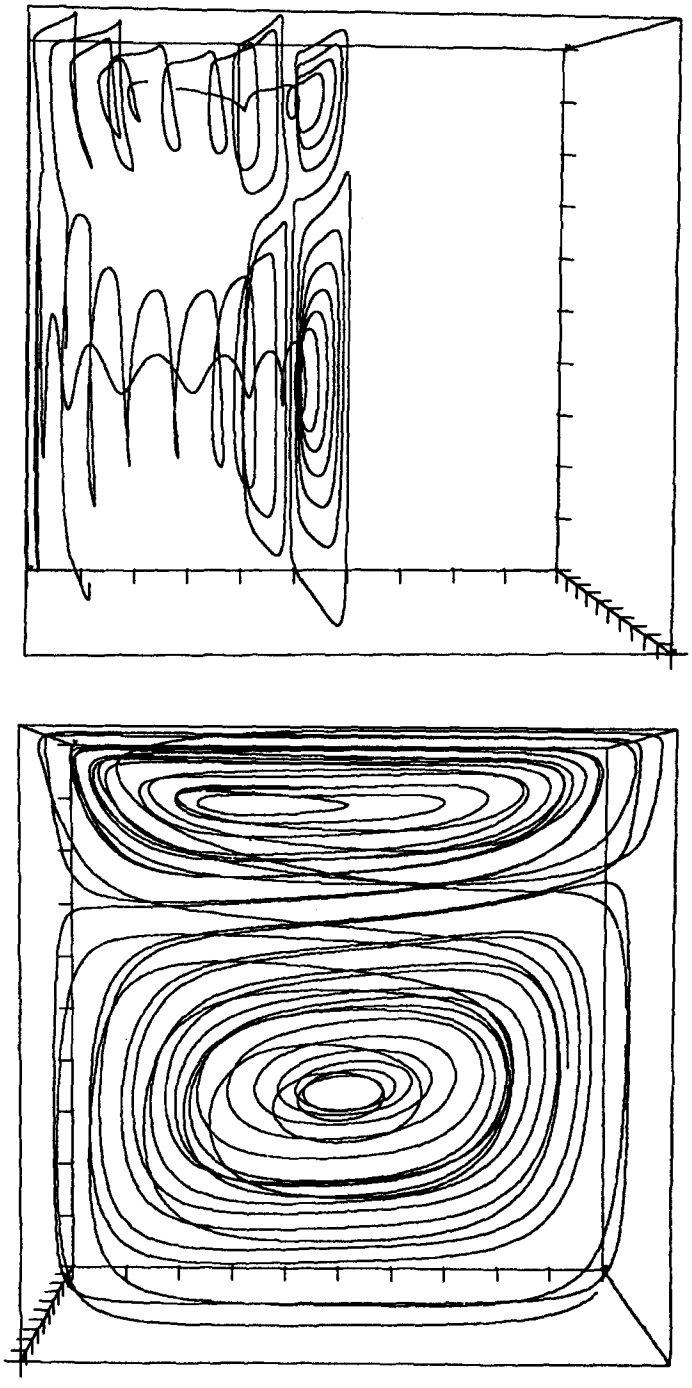

Figure 6. Flow structure (Ra = 10,000, Ma = −1000).

to the increasing role played by the bulk buoyancy forces that gradually overcome the effect of surface tension on the top side of the cavity.

Case (D) $Ra = 10^3$, $Ma = -10^3$ and Case (E) $Ra = 10^4$, $Ma = -10^3$. In these two cases, due to the negative value of Marangoni number, there is an opposition of effects between buoyancy and surface tension. For this reason, it is possible to clearly distinguish the effect of the two different contributions. In figures 5(a) and (b), case (D), we can clearly see that the Marangoni effect is confined in the upper roll, which is counter-rotating with respect to cases (A), (B) and (C). The effect of buoyancy is confined in the lower double vortex which, as can be seen for case (D), is confined to a small region of the fluid domain. On the contrary to case (A) (Ra = 0, Ma = 1000), the main direction of the flow in the lower secondary vortex is from the end-wall to the centre of the cavity. This is due to the opposite direction of rotation of the lower vortex and to the consequent opposite sign of ω_3. It is noted that although these results can not be quantitatively compared to the two-dimensional experiments of Villers & Platten (1987), qualitatively they indicate similar counter-rotating vortices. Case (E) (Ra = 10,000, Ma = −1000) shows an increasing effect of buoyancy and as a consequence, a growth of the buoyancy driven lower vortex, figures 6(a) and (b). Also in this case, it is clearly evident how the flow is strongly divided into two regions. The upper one where the motion is induced by surface tension and the lower one driven by buoyancy.

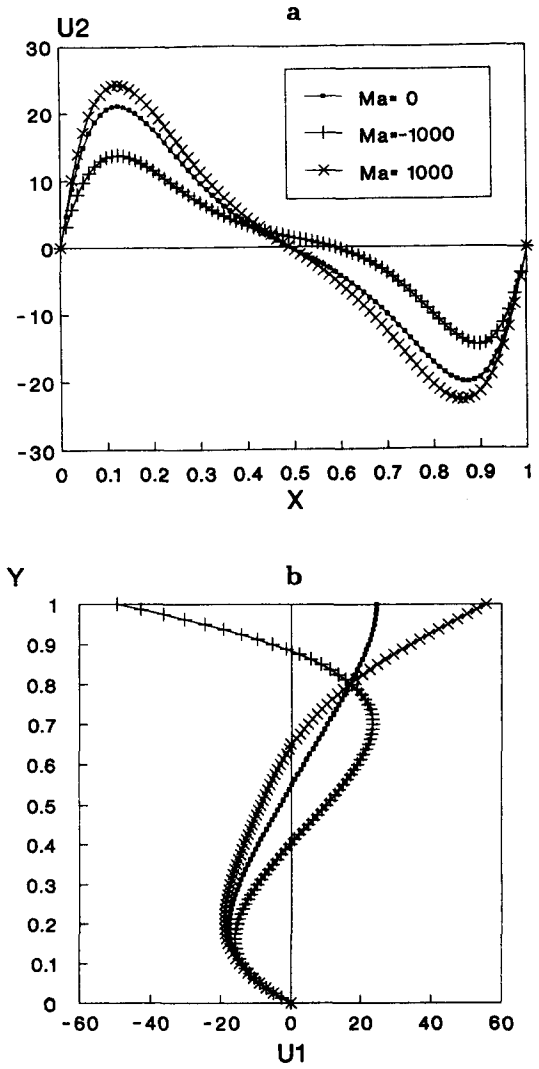

Figure 7. Velocity profiles on the cavity mid-plane ($z = 0.5$) for various Ma and Ra = 10,000.

The u_1 and u_2 velocity profiles on the cavity centreline are plotted in figures 7(a) and (b) in order to clearly show positive and negative Marangoni number effects.

5.2. Thermal field

The temperature distribution confirms the general behaviour discussed above. In particular, from the isotherm plots on the cavity mid-plane (i.e. $z = 0.5$) shown in figure 8, the following can be noted:

(i) For positive Ma there is a strong thermal boundary layer located close to the upper-right corner due to the effect of thermocapillary convection in the vicinity of the free surface, see figures 8(a) and (b).

(ii) For Ma = 1000 and Ra = 10,000 the convection influences also the bulk of the fluid inducing a horizontal thermal inversion. This phenomenon is similar to the one that was found by Mallinson & de Vahl Davis (1976) in the standard double-glazing window problem at Ra = 100,000.

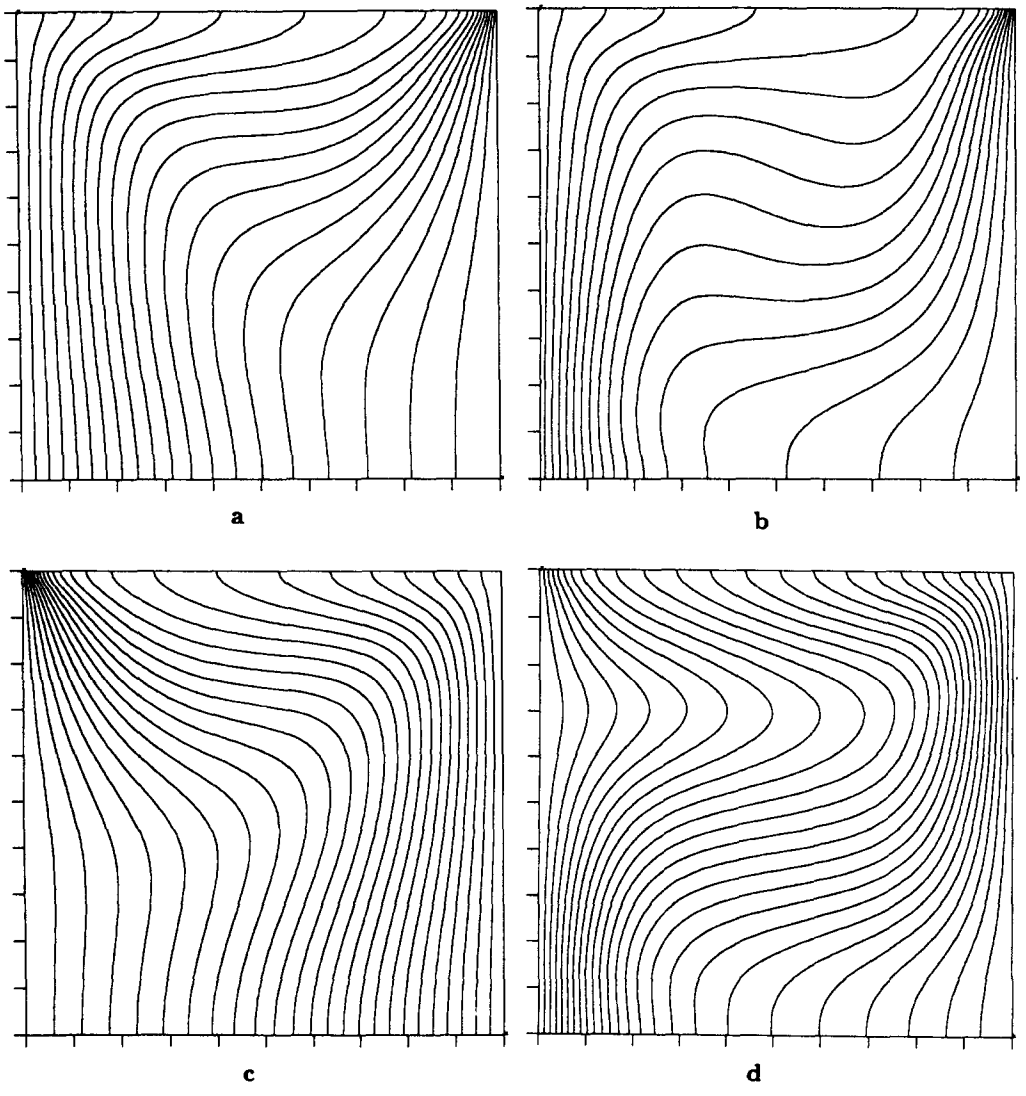

Figure 8. Isotherms on the cavity mid-plane ($z = 0.5$). (a) Ra = 0; Ma = 1000; (b) Ra = 10,000, Ma = 1000; (c) Ra = 1000, Ma = −1000; (d) Ra = 10,000, Ma = −1000.

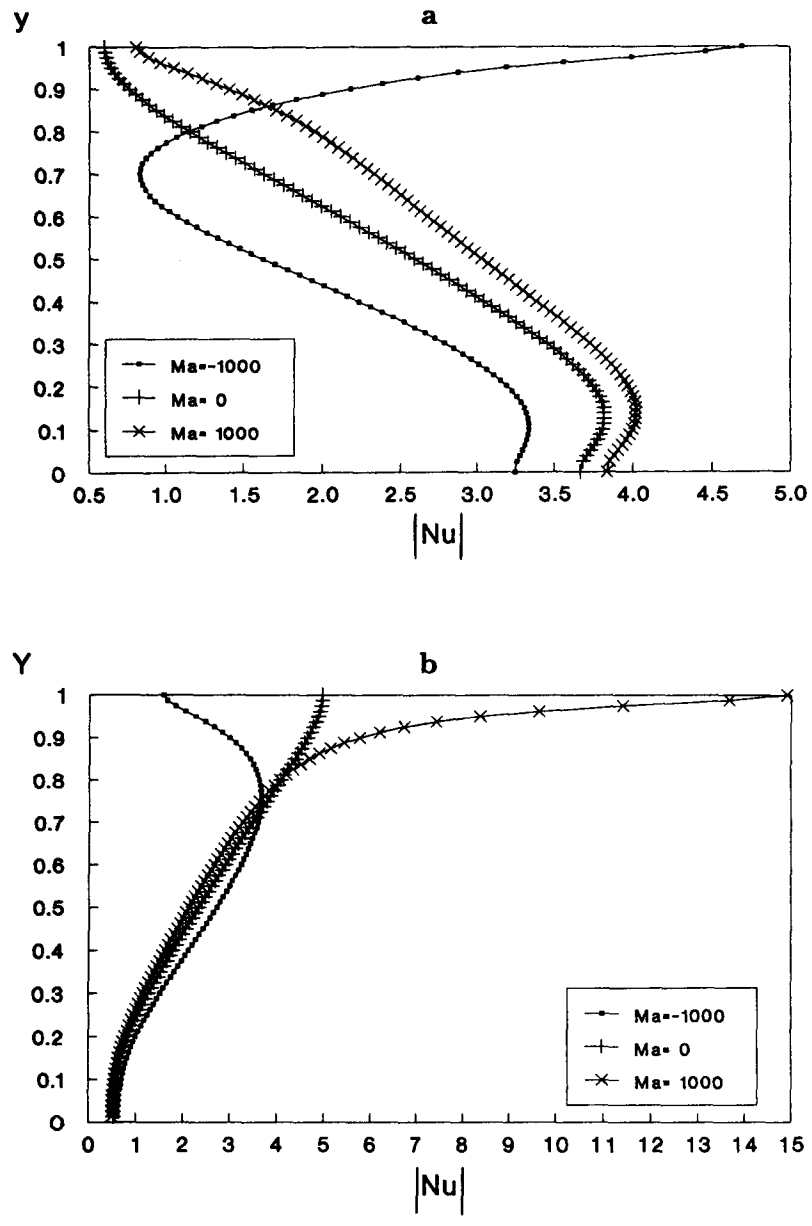

Figure 9. Local Nusselt number on the hot (a) and cold (b) walls for various Ma and Ra = 10,000.

(iii) The negative Ma causes a strong penetration of hot fluid in the centre of the cavity due to the combined effect of the two counter-rotating recirculations, see figure 8(d).

The behaviour of the thermal boundary layers on the hot and cold walls at Ra = 10,000 as a function of Ma is well described by the local Nusselt number plots shown in figures 9(a) and (b). The absolute value of local Nusselt number distribution on the hot wall is shown for Ma = -1000, 0 and $+1000$. It is noted that negative Ma clearly yields a different Nu distribution, in particular the minimum of Nu = 0.827 is located at $y = 0.7$ instead of $y = 1$ for the other two parameter values. However, it is noted that on the cold wall [see figure 9(b)], for negative Ma the extreme is Nu = 3.672 at $y = 0.762$. The shape of the Nu curves at Ma = -1000 is due to the double vortex structure discussed above. The local Nu at Ma = 1000 in figure 9(b) reaches a value of 15 confirming the presence of a very steep boundary layer in the upper downstream corner noted in item (i) above. The averaged Nusselt number vs Ma with Ra as parameter (see figure 10) shows

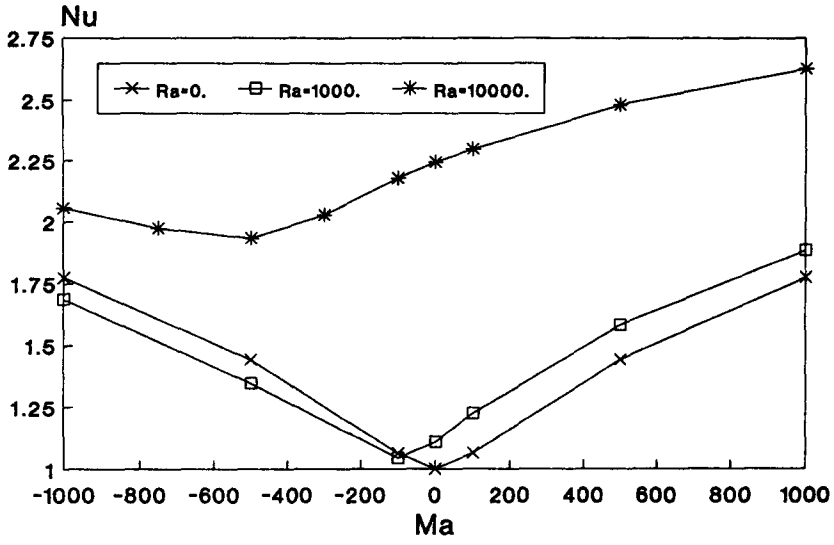

Figure 10. Average Nusselt number for different values of Ma and Ra.

a shift in the position of the minimum Nu due to the counteracting superposition of the surface tension and buoyancy effects.

6. CONCLUSIONS

A three-dimensional numerical study of combined buoyancy and thermocapillary convection in a liquid with a Prandtl number of 7 is presented.

For the case of positive Marangoni number the fluid structure is mainly constituted by a dominant core vortex structure which becomes stronger as either of the independent parameters (Ra and Ma) are increased.

More complex and interesting is the flow structure for negative values of Marangoni number. In this case, the fluid is stratified and flow field is clearly divided into two separate regions where the motion is driven by thermocapillary (upper region) and buoyancy (lower region) respectively.

Also temperature distribution as well as the local Nusselt number is strongly modified by the presence of thermocapillary effects leading to unexpected critical regions for heat exchange.

For the range of parameters considered here, it was noted that the flow is steady. However, it is expected that for a higher range of values instabilities will appear and a transition to unsteadiness will occur.

Acknowledgement—Partial financial support was provided to the first author (M.B.) by the University of Rome for which the authors are grateful.

REFERENCES

AFRID, M. & ZEBIB, A. 1990 Oscillatory three-dimensional convection in rectangular cavities and enclosures. *Phys. Fluids* **A2,** 1318–1327.

BABU, V. & KORPLEA, S. A. 1990 Three-dimensional thermocapillary convection in a cavity. *Computers Fluids* **18,** 229–238.

BEHNIA, M. & DE VAHL DAVIS, G. 1990 Fine mesh solutions using stream function-vorticity formulation. *Notes Numerical Fluid Mech.* **27,** 11–18.

BEHNIA, M., DE VAHL DAVIS, G., STELLA, F. & GUJ, G. 1990 A comparison of velocity–vorticity and stream function-vorticity formulations for Pr = 0. *Notes Numerical Fluid Mech.* **27,** 19–24.

BERGMAN, T. L. & KELLER, J. R. 1988 Combined buoyancy, surface tension flow in liquid metals. *J. Num. Heat Transfer* **13,** 49–63.

BERGMAN, T. L. & RAMADHYANI, S. 1986 Combined buoyancy and thermocapillary driven convection in open square cavities. *J. Num. Heat Transfer* **9,** 441–451.

DAVIS, S. H. 1987 Thermocapillary instabilities. *A. Rev. Fluid Mech.* **19,** 403–435.

GEBHART, B., JALURIA, Y., MAHAJAN, R. L. & SAMMANIKIA, B. 1988 *Buoyancy-induced Flows and Transport.* Hemisphere, New York.

GUJ, G. & STELLA, F. 1988 Numerical solution of high-Re recirculating flows in vorticity–velocity form. *Int. J. Numer. Meth. Fluids* **8,** 405–416.

LEBON, G. 1984 Recent developments in surface-tension driven instabilities. *Acta Astronautica* **11,** 353–359.

LIMBOURG-FONTAINE, M. C., PÉTRÉ, G. & LEGROS, J. C. 1985 Texus 8 experiment: effects of a surface tension minimum on thermocapillary convection. *Physico-Chem. Hydrodynamics* **6,** 301–312.

MALLISON, G. & DE VAHL DAVIS, G. 1973 The method of the false transient for the solution of coupled elliptic equations. *J. Comp. Phys.* **12,** 435–461.

MALLISON, G. & DE VAHL DAVIS, G. 1976 Three dimensional natural convection in a box: a numerical study. *J. Fluid Mech.* **83,** 11–21.

MYSHKIS, A. D., BABSKII, V. G., KOPACHEVSKII, N. D., SLOBOZHANIN, L. A. & TYUPTSOV, A. D. 1986 Low gravity fluid mechanics. Springer, Berlin.

PÉTRÉ, G., LIMBOURG-FONTAINE, M. C. and LEGROS, J. C. 1983 Study of the surface tension minimum of aqueous alcohol solutions and movements at the interface air-solution. *Proc. 4th Europ. Symp. Mat. Sci. Microgravity*, European Space Agency, Madrid, pp. 199–200.

PLATTEN, J. K., VILLERS, D. & LHOST, O. 1988 L.D.V. study of some free convection problems at extremely slow velocities: Soret driven convection and Marangoni convection. *Laser Anemometry in Fluid Mechanics, III* (Edited by ADRIAN, R. J., ASANUMA, T., DURAO, D. F. G., DURST, F. & WHITELAW, J. H.), Istituto Superior Technico, Lisbon.

RAMANAN, N. & KORPELA, S. A. 1990 Thermocapillary convection in an axi-symmetric pool. *Computers Fluids* **18,** 205–215.

SAMARSKII, A. & ANDREYEV, V. 1963 On a high-accuracy difference scheme for elliptic equation with several space variables. *USSR Comp. Maths. Math. Phys.* **3,** 1373–1382.

SCHWABE, D. 1981 Marangoni effects in crystal growth melts. *Physico-Chem. Hydrodynamics* **2,** 263–280.

SCRIVEN, L. E. & STERLING, C. V. 1960 The Marangoni effects. *Nature* **187,** 186–188.

SMITH, M. K. & DAVIS, S. H. 1983 Instabilities of dynamic thermocapillary liquid layers, part 1. Convective instabilities. *J. Fluid Mech* **132,** 119–144.

STELLA, F. & GUJ, G. 1992 Parallel solver for three dimensional viscous flows. In *Parallel Computing: Problems, Methods and Applications* (Edited by MESSIMA, P. & MUNLI, A.), pp. 389–401. Elsevier Science, Amsterdam.

VILLERS, D. & PLATTEN, J. K. 1985 Marangoni convection in systems presenting a minimum in surface tension. *Physico-Chem. Hydrodynamics* **6,** 435–451.

VILLERS, D. & PLATTEN, J. K. 1987 Separation of Marangoni convection from gravitational convection in earth experiments. *Physico-Chem. Hydrodynamics* **8,** 173–183.

ZEBIB, A., HOMSY, G. M. & MEIBURG, E. 1985 Marangoni convection in a square cavity. *Phys. Fluids* **28,** 3467–3476.